Constrained density functional theory calculation with iterative optimization

Daniel Kidd, A. S. Umar, and Kálmán Varga*
Department of Physics and Astronomy, Vanderbilt University, Nashville, Tennessee 37235, USA

(Received 14 June 2018; published 6 August 2018)

An iterative optimization approach that simultaneously minimizes the energy and optimizes the Lagrange multipliers enforcing desired constraints is presented. The method is tested on previously established benchmark systems and it is proved to be efficient and accurate. The approach can also be efficiently used when the constraint is not a scalar quantity but a spatially varying function such as the charge density distribution.

DOI: 10.1103/PhysRevB.98.075108

I. INTRODUCTION

Density functional theory (DFT) [1] is one of the most important approaches to calculating ground-state properties in molecules and solids. The extension of DFT for ground-state calculations in constrained systems (cDFT) [2–6] opened a new venue for the description of charge excitations [7], magnetic transitions [8], spin dynamics [9], and electron transfer [10]. This technique became a more powerful tool with a greatly enhanced range of applicability through the introduction of a self-consistent formulation by Wu and Van Voorhis [11]. It is now implemented in many computer codes using localized basis sets (NWCHEM [11], QCHEM [12,13], SIESTA [14], DEMON2K [15], ADF [16]), plane waves (CPMD [17], QUANTUMESPRESSO [18], VASP [19]), density matrices (CONQUEST [20]), wavelets (BIGDFT [21]), and projector augmented wave (PAW) methods [22].

Armed with these powerful computational tools, the cDFT has been intensively used (see a recent review in Ref. [23]) in a wide variety of problems including electron transfer reactions [24–28], excitation energy transfers [29], calculation of coupling parameters [30], and noncollinear magnetism [19]. Computational approaches using local constraints [31], orthogonality conditions [32], and constrained orbitals [33] have also been developed.

In the direct optimization approach of Wu and Van Voorhis [11], a constraint is added to the energy functional using the Lagrange multiplier method. The Lagrange multiplier determines the constraining potential, but it is not explicitly known. Wu and Van Voorhis have shown that the functional is a strictly concave function of the Lagrange multiplier and there is a unique stationary point which is a maximum. They proposed a nested-loop approach with an outer self-consistent loop (a normal DFT loop) and an inner constraint loop. The constraint loop determines the Lagrange multiplier aided by the first and the second derivatives of the functional. The constraint iterations are relatively cheap using localized orbitals (the cost is a diagonalization of the Hamiltonian), but in the case of plane-wave or real-space grid codes describing larger systems, this step can be a bottleneck.

In this paper, we implement an approach that simultaneously minimizes the energy and optimizes the Lagrange multipliers to satisfy the constraints. The method uses steepest-descent iteration for the orbitals and the Lagrange multiplier is iteratively updated in each step. The Lagrange multiplier is adjusted in each iteration in order to enforce the constraining condition [34,35] on the desired expectation value. The advantage of the approach is that it can be easily implemented alongside steepest descent or conjugate gradient minimization, allowing efficient cDFT calculations using real-space grids. A distinctive merit of the method is that it can also be used to enforce spatially varying constraints. One can constrain not only a prescribed total charge in a region, but a desired density distribution can also be enforced, opening new possible applications for cDFT.

In Sec. II, we outline the main points of the formalism, leaving the details collected in the Appendices. In Sec. III, numerical tests are presented. The last section is a short summary. Two appendices are added that describe the iterative diagonalization formalism, give an overview of the Lagrange multiplier approach, and motivate the iterative optimization.

II. FORMALISM

A. Constrained density functional theory

In DFT, the total energy in atomic units (a.u.) is given by

$$E[\rho] = T + \int d\mathbf{r}\, v_n(\mathbf{r})\rho(\mathbf{r}) + J[\rho] + E_{\rm xc}[\rho^\alpha, \rho^\beta], \quad (1)$$

where

$$T = \sum_{\sigma}^{\alpha,\beta} \sum_{i}^{N_\sigma} \langle \psi_{i\sigma}| -\frac{1}{2}\nabla^2 |\psi_{i\sigma}\rangle \quad (2)$$

is the kinetic energy, J is the Coulomb energy, $E_{\rm xc}$ is the exchange-correlation energy, $v_n(\mathbf{r})$ is the external potential, and

$$\rho^\sigma(\mathbf{r}) = \sum_{i}^{N_\sigma} |\psi_{i\sigma}(\mathbf{r})|^2 \quad (3)$$

*kalman.varga@vanderbilt.edu

is the electronic density for spin $\sigma = \uparrow, \downarrow$ of N_σ electrons ($\rho = \rho^\uparrow + \rho^\downarrow$). A generic constraint can be defined as

$$\sum_{\sigma}^{\alpha,\beta}\sum_{i}^{N_\sigma}\langle\psi_{i\sigma}|\hat{Q}^\sigma|\psi_{i\sigma}\rangle = Q_0, \tag{4}$$

where $\hat{Q}^\sigma(\mathbf{r})$ is an operator and Q_0 is a desired expectation value. For example, it is very common to constrain the charge density so that there is a specified number of electrons for each spin, N_c^σ, within a certain region of space:

$$\int w_c^\sigma(\mathbf{r})\rho^\sigma(\mathbf{r})d\mathbf{r} = N_c^\sigma. \tag{5}$$

Here, $w_c^\sigma(\mathbf{r})$ is a weighting function confining the electron density into a specified spatial region [e.g., $w_c^\sigma(\mathbf{r})$ is equal to 1 within a certain volume and 0 elsewhere].

In order to minimize the total energy of Eq. (1) subject to the constraint of Eq. (4), a functional is defined to be

$$L[\rho,\lambda] = E[\rho] + \lambda\left(\sum_{\sigma}^{\alpha,\beta}\sum_{i}^{N_\sigma}\langle\psi_{i\sigma}|\hat{Q}^\sigma|\psi_{i\sigma}\rangle - Q_0\right), \tag{6}$$

where λ is the Lagrange multiplier.

Minimizing L with respect to λ forces the constraint to be satisfied. By making this functional stationary under the condition that the Kohn-Sham orbitals are orthonormalized (see Appendix B and the discussion in Ref. [36]), one gets the Kohn-Sham equations with an extra term, i.e., the constraining potential $\lambda Q^\sigma(\mathbf{r})$,

$$\left[\hat{H}_{\mathrm{KS}}^\sigma + \lambda Q^\sigma(\mathbf{r})\right]\psi_i^\sigma(\mathbf{r}) = \epsilon_i\psi_i^\sigma(\mathbf{r}). \tag{7}$$

Here,

$$\hat{H}_{\mathrm{KS}}^\sigma = -\frac{1}{2}\nabla^2 + v_n(\mathbf{r}) + v_{\mathrm{xc}}^\sigma(\mathbf{r}) + \int\frac{\rho(\mathbf{r}')}{|\mathbf{r}-\mathbf{r}'|}d\mathbf{r}', \tag{8}$$

where v_{xc}^σ is the exchange and correlation potential. Up until now, the popular notation of the literature has been followed; however, from now on, we drop the spin index for simplicity and assume that each orbital is doubly occupied.

For a given λ, one can determine the orbitals and, with the correct λ, the constraint is fulfilled. Wu and Van Voorhis [11] have established a means of solving for a unique stationary point. They have shown that $L(\rho,\lambda)$ is a strictly concave function of λ, with only one stationary point which is a maximum. Both the first and second derivatives of L with respect to λ can be derived, so the optimization can be done efficiently. Finding λ requires the solution of Eq. (7) for a given λ and updating λ, thus optimizing L (see Appendix B 2). The desired constraining potential is found when the constraining equation is satisfied with respect to a prescribed accuracy. Further discussion on the optimization of constrained DFT can be found in Ref. [36], in which efficient calculations involving multiple constraints are described.

B. Iterative minimization

We will use a method that is based on iterative diagonalization. This approach is often used in cases of large basis dimension, such as for the three-dimensional real-space grid representation, where direct diagonalization of the Hamiltonian matrix is infeasible and alternate methods must be used to determine the lowest-energy eigensolutions. The simplest approach is a steepest-descent iteration,

$$\psi_j^{(n+1)}(\mathbf{r}) = \mathcal{O}\left\{\psi_j^{(n)}(\mathbf{r}) - x_0\left(\hat{H}_{\mathrm{KS}} - \epsilon_j^{(n)}\right)\psi_j^{(n)}(\mathbf{r})\right\}. \tag{9}$$

Here, $x_0 = \Delta t/\hbar$,

$$\epsilon_j^{(n)} = \left\langle\psi_j^{(n)}\middle|\hat{H}_{\mathrm{KS}}\middle|\psi_j^{(n)}\right\rangle, \tag{10}$$

and $\mathcal{O}$ indicates Gram-Schmidt orthonormalization, which is required to preserve the orthonormality of the single-particle states at each update step. The starting wave function $\psi_j^{(n)}$ is some initial guess, e.g., linear combination of atomic orbitals, and x_0 is chosen to be sufficiently small for convergence. The steepest-descent step can be derived from imaginary-time propagation and can be improved by using higher-order approximations to the exponential operator (see Appendix A).

C. Iterative minimization with a constraint

The advantage of the iterative diagonalization is that it can be combined with a step which is designed to enforce the constraints. The motivation for the concrete form of the iterative updates, the possible implementations, and the highlights of earlier works are summarized in Appendix B.

In the case of constraint, the goal is to update each orbital towards the minimum-energy configuration while maintaining that an arbitrary expectation value, related to an associated operator $\hat{Q}$, does not change from one static iteration to the next, i.e.,

$$\sum_j\left\langle\psi_j^{(n+1)}\middle|\hat{Q}\middle|\psi_j^{(n+1)}\right\rangle = \sum_j\left\langle\psi_j^{(n)}\middle|\hat{Q}\middle|\psi_j^{(n)}\right\rangle. \tag{11}$$

Furthermore, the value of this expectation value is meant to match a given input value,

$$\sum_j\left\langle\psi_j^{(n+1)}\middle|\hat{Q}\middle|\psi_j^{(n+1)}\right\rangle = Q_0. \tag{12}$$

These conditions may be incorporated into the above iterative formalism by the inclusion of a Lagrange multiplier constraint term such that the update scheme becomes

$$\psi_j^{(n+1)}(\mathbf{r}) = \mathcal{O}\left\{\psi_j^{(n)}(\mathbf{r}) - x_0\left(\hat{H}_{\mathrm{KS}} + \lambda^{(n)}\hat{Q} - \epsilon_j^{(n)}\right)\psi_j^{(n)}(\mathbf{r})\right\}. \tag{13}$$

In this update scheme, one has to simultaneously iterate the Lagrange multiplier $\lambda^{(n)}$. The simplest choice is to use a steepest-descent iteration for λ as well (see Appendix B 3), but one can work out a much better scheme by choosing $\lambda^{(n)}$ in such a way that the constraint in Eq. (11) is satisfied.

To this end [34,35], one includes an intermediate step,

$$\psi_j^{(n+1/2)}(\mathbf{r}) = \mathcal{O}\left\{\psi_j^{(n)}(\mathbf{r}) - x_0\left(\hat{H}_{\mathrm{KS}} + \lambda^{(n)}\hat{Q} - \epsilon_j^{(n)}\right)\psi_j^{(n)}(\mathbf{r})\right\}. \tag{14}$$

The difference of the relevant expectation value between the original and half steps is calculated,

$$\delta Q = \sum_j\left\langle\psi_j^{(n+1/2)}\middle|\hat{Q}\middle|\psi_j^{(n+1/2)}\right\rangle - \sum_j\left\langle\psi_j^{(n)}\middle|\hat{Q}\middle|\psi_j^{(n)}\right\rangle, \tag{15}$$

so that the Lagrange multiplier may be updated as

$$\lambda^{(n+1)} = \lambda^{(n)} + c_0 \frac{\delta Q}{2x_0 \sum_j \langle \psi_j^{(n)} | \hat{Q}^2 | \psi_j^{(n)} \rangle + d_0} + \frac{\sum_j \langle \psi_j^{(n)} | \hat{Q} | \psi_j^{(n)} \rangle - Q_0}{2x_0 \sum_j \langle \psi_j^{(n)} | \hat{Q}^2 | \psi_j^{(n)} \rangle + d_0}. \quad (16)$$

Here, c_0 and d_0 are numeric constants; their role is explained in Appendix B 4. A good choice for c_0 is a value between 0.9 and 1.0, and that for d_0 is around 7×10^{-5}. In the above equation, λ is corrected with two terms. The first correction seeks to preserve the expectation value of $\hat{Q}$ by reducing the change in δQ [see Eq. (B30)]. The second correction term adjusts the expectation value toward the desired value [see Eq. (B29)].

With these readjustments, the $(n+1)$th step is given as

$$\psi_j^{(n+1)}(\mathbf{r}) = \mathcal{O}\{\psi_j^{(n+1/2)}(\mathbf{r}) - x_0(\lambda^{(n+1)} - \lambda^{(n)} + \delta\lambda)\hat{Q}\psi_j^{(n+1/2)}(\mathbf{r})\}. \quad (17)$$

This update step can be considered as a simultaneous correction meant to preserve the expectation value as well as force the expectation value to be equal to a desired quantity. The numerical constants appearing in the iteration play a similar role to the density mixing parameters in the self-consistent solution of the Kohn-Sham equations by helping the speed of convergence. The motivation and details of the above steps for the simultaneous diagonalization of the Hamiltonian and the optimization of λ are given in Appendix B 4.

This update scheme settles the Kohn-Sham system into the minimum-energy state while maintaining a constraint on an arbitrary state expectation value. Effectively, what occurs is the convergence of the Kohn-Sham system towards the global ground state for a total effective potential which is iteratively updated simultaneous to the orbitals. Thus, the final state may be fully constructed by real-valued orbitals, and the converged Lagrange multiplier term $\lambda^{\text{final}} Q$ represents a fictitious, additional external potential which corresponds to a Kohn-Sham state exhibiting the desired expectation value.

III. RESULTS

In this section, we present results of the iterative constraint update scheme. In each case, a real-space grid representation was used alongside a finite-difference representation of the kinetic energy. The ion cores were treated using norm-conserving Troullier and Martins pseudopotentials [37].

A. Simple model system

As a simple numerical test, we consider a three-dimensional harmonic oscillator $V(\mathbf{r}) = \frac{1}{2}\omega^2\mathbf{r}^2$ (a.u.) with $N = 5$ orbitals, subject to the constraint

$$Q - Q_0 = 0, \quad (18)$$

where

$$Q = \sum_{j=1}^{N} \langle \psi_j^{(n)} | \mathbf{r}^2 | \psi_j^{(n)} \rangle. \quad (19)$$

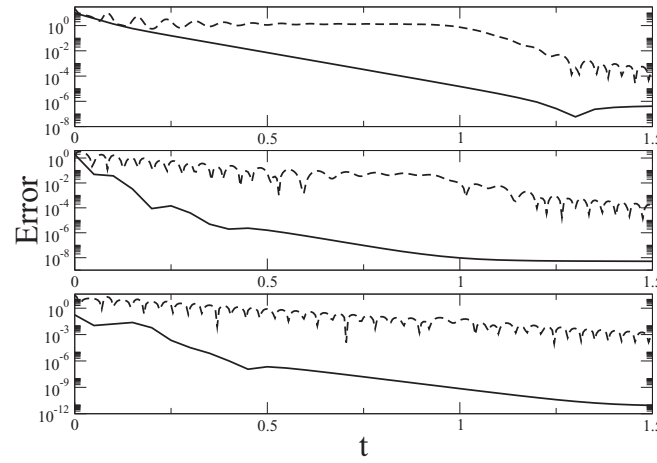

FIG. 1. Convergence of energy (top), Lagrange multiplier λ (middle), and Q (bottom) as a function of time (in a.u.) for a simple steepest-decent update (dashed line, $x_0 = 0.0005$ a.u.) and the λ optimization (solid line, $x_0 = 0.005$ a.u.).

In the test calculation, the parameters ω and Q_0 are chosen to be 1 and 25 a.u., respectively. The model is analytically solvable. Adding the λQ term to the Hamiltonian is equivalent to a modified harmonic-oscillator potential with $\omega' = \sqrt{\omega^2 + \lambda}$. The square radius of a harmonic-oscillator wave function with quantum numbers (n_x, n_y, n_z) is equal to $\frac{1}{2\omega}(2n_x + 2n_y + 2n_z + 3)$, so the condition $Q_0 = 25$ determines the analytical value of λ and the energy. The numerical solution for a simple steepest-descent update and the λ optimization approach presented in the previous section are compared in Fig. 1. The figure shows that the λ optimization is very accurate, both in energy and in constraining Q, and the λ convergence is very fast. The steepest-descent approach, based on Eqs. (B22) and (B23), also works but the accuracy is orders of magnitude worse. This simple, but clean example (no self-consistency) shows that the λ optimization approach is accurate and fast.

B. Charge constraint

Now we apply the iterative optimization scheme to charge transfer systems studied by Wu and Van Voorhis [11,25]. They used a weight function $w(\mathbf{r})$, which designates coordinate space belonging to the donor with a value of 1 and that of the acceptor with a value of -1. In this way, a Lagrange multiplier term is added to the Kohn-Sham equation as $\lambda Q = \lambda w(\mathbf{r})$, effectively representing a step potential which may be tuned during optimization until the desired charge imbalance between the two partitions,

$$N_c = Q_0 = \sum_{j=1}^{N} \langle \psi_j^{(n)} | w(\mathbf{r}) | \psi_j^{(n)} \rangle = \int w(\mathbf{r})\rho(\mathbf{r})d\mathbf{r}, \quad (20)$$

is reached. The weight function may be defined using a scheme such as Hirshfeld partitioning [38,39] such that

$$w(\mathbf{r}) = \frac{\sum_{i\in D} \rho_i(\mathbf{r} - \mathbf{R}_i) - \sum_{i\in A} \rho_i(\mathbf{r} - \mathbf{R}_i)}{\sum_i \rho_i(\mathbf{r} - \mathbf{R}_i)}, \quad (21)$$

where $\rho_i(\mathbf{r})$ represents the unperturbed electron density of ion i and $\mathbf{R}_i$ is its location.

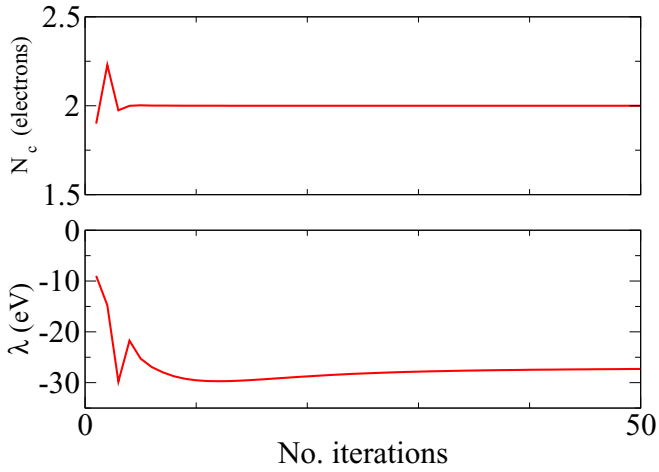

FIG. 2. Convergence of charge difference (top) and Lagrange multiplier (bottom) for a N_2 molecule. The input desired charge difference was $N_c = 2$ electrons.

In our formalism, we choose the weight function of Eq. (21) to be the operator whose associated expectation value N_c is being constrained to a given value. In this way, we are able to perform charge constraint optimization in DFT using a real-space grid approach which, unlike the atomic orbitals basis, does not allow for a practical means of storing the full Hamiltonian matrix and, instead, relies on algorithms which describe the action of the Hamiltonian matrix on a wave-function vector. Furthermore, in this update scheme, one is not required to use a nested-loop form in which either the energy minimization or the constraint condition is satisfied via an inner loop, while the other is satisfied using the outer loop. In the iterative constraint method, one progresses towards the stationary point by simultaneously updating each. This may lead to significantly faster run times or enhanced stability.

One of the simplest cases to consider is the diatomic N_2 molecule. Here, one atom is designated as the donor and the other is the acceptor. The above-described procedure was carried out for a desired charge difference between the two atoms of $N_c \to 2$ electrons. The width of the computational box was 6 Angstroms on each side with 25 grid points along each axis. A plot of the convergence of N_c and of the Lagrange multiplier λ is presented in Fig. 2. We find that only a small number of iterations is needed for satisfactory convergence in this case. The resulting value for λ, indicating the depth of the step potential enforcing the charge difference, was -27.01 eV. The electron density for the N_2 molecule using conventional DFT is shown in Fig. 3(a) and that of the charge constrained N_2 molecule is shown in Fig. 3(b). By including an additional potential of -27.01 eV $\times\, w(\mathbf{r})$ in a conventional DFT calculation of the N_2 molecule, the charge difference of $N_c = 2$ electrons naturally arises and the density, shown in Fig 3(c), nearly exactly matches that of the constrained DFT case.

We next consider the small systems tested by Wu and Van Voorhis in Table 1 of Ref. [25]. For long separation distances between the donor and acceptor molecules, $\mathbf{R}$, one would expect that the energy varies as $1/\mathbf{R}$. A good test of the energies calculated by a charge constraint DFT program would be to

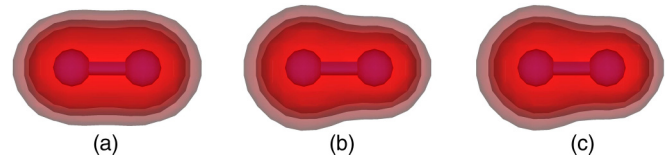

FIG. 3. Converged electron density of a N_2 molecule calculated using (a) conventional DFT, (b) constrained DFT with an imposed charge difference of two electrons, and (c) conventional DFT with an additional external potential of -27.01 eV $\times\, w(\mathbf{r})$. Three isosurfaces corresponding to the density of 0.33, 0.67, and 1.0 Å^{-3} are shown.

plot the total energy vs $1/\mathbf{R}$ and show the expected linear dependence. Furthermore, one may use the slope of this curve in order to determine the total energy of the charge-separated (CS) system, i.e., $\mathbf{R} \to \infty$. Since at an infinite separation distance the two molecules should be independent of one another, this total energy should equal the sum of separate calculations for the appropriately ionized donor and acceptor molecules, that is D^- and A^+ in the case of $N_c = 2$.

An example trend of the total energy vs $1/\mathbf{R}$ is presented in Fig. 4 for the system N_2^-–N_2^+ and a charge difference of $N_c = 2$. The data is well fit by a linear trend line. The slope indicates an expected CS total energy of -1069.735 eV. This value is in good agreement with the total energy of separate calculations for the N_2^+ and N_2^- molecules, which is -1070.970 eV. These values, as well as those for the cases of H_2O^-–F_2^+ and $C_2F_4^-$–$C_2H_4^+$, are presented in Table I. We note that each value for $(E_{D^-} + E_{A^+})$ is higher than its E_{CS} counterpart by about 1.15 eV. Apart from this small systematic shift, all values agree well, indicating that these long-range charge transfer states are being well represented by the present scheme. We note that the reported values in Table I do not represent total energies of these systems. This is due to the fact that pseudopotentials have been employed and the frozen-core approximation energies, corresponding to the pseudopotential contributions, have been neglected. In principle, because the difference in total energy is nearly always the desired calculated quantity,

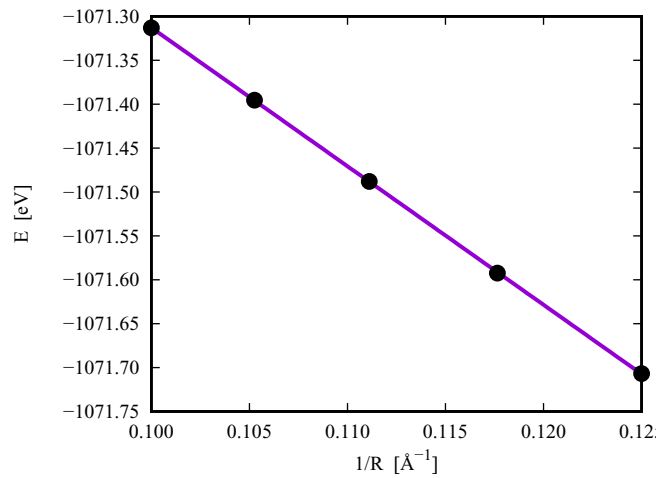

FIG. 4. Total-energy calculations using charge difference constrained DFT to describe the system N_2^+–N_2^- for five separation distances $\mathbf{R}$ chosen within a range of 8 to 10 Å.

TABLE I. The charge-separated state energy E_{CS} for three small molecule cases, determined using a linear fit of five data points representing the total energy found using a charge difference constraint of $N_c = 2$ for separation distances ranging between 8 and 10 Angstroms. These values are compared to the sum of individual calculations for each constituent ionized molecule.

D	A	E_{CS}	$(E_{D^-} + E_{A^+})$	% diff.
N_2^-	N_2^+	−1069.735	−1070.970	0.115
H_2O^-	F_2^+	−1767.172	−1768.204	0.058
$C_2F_4^-$	$C_2H_4^+$	−3323.066	−3324.250	0.036

one may compare such valence energies among like systems, represented using the same pseudopotentials, as if they were the true total energies.

Finally, we investigate the popular charge transfer excitation in zincbacteriochlorin-bacteriochlorin (ZnBC-BC). This system is a common component of suggested light-harvesting devices, appearing with a phenylene link. However, it has been demonstrated that ignoring the link introduces negligible error [40]; therefore, the pair of isolated molecules separated by 5.84 Å is commonly studied. The charge transfer excited state of this complex was of the earliest shown to be misrepresented by time-dependent density functional theory (TDDFT) [40], due to an incorrect treatment of the long-range exchange potential. Thus, there are many studies devoted to the correction of this shortcoming. Such calculations include TDDFT using various local [40–42] and hybrid [42] functionals, methods combining a configuration-interaction singles (CIS) approach [40,43], and also use of the Bethe-Salpeter formalism [44]. The cDFT formalism of Wu and Voorhis was also initially applied to this system [11,25], using an atomic orbitals basis, specifically the 6–31 G* basis set, and the Becke-Lee-Yang-Par (BLYP) functional [45,46]. This approach has also been recently tested on the ZnBC-BC complex using a flexible Daubechies wavelet basis and the local density approximation (LDA) functional [47].

The difference of the DFT-calculated ground-state density for ZnBC-BC and the charge constrained DFT density is shown in Figs. 5(a) and 5(b) for the cases of $ZnBC^+$–BC^- and $ZnBC^-$–BC^+, respectively. The LDA relaxed coordinates were provided by Ratcliff *et al.* of Ref. [47]. The energy values for this large system maintain a linear dependence with regards to $1/\mathbf{R}$, as shown in Fig. 6. The energies of the two excited states relative to the neutral ground state, using a separation distance of $\mathbf{R} = 5.84$ Å, were determined to be 3.54 eV for $ZnBC^+$–BC^- and 3.95 eV for $ZnBC^-$–BC^+. The latter value agrees well with previously calculated values (3.91 eV [40], 3.94 eV [11], and 3.98 eV [47]), while the former is lower than similar studies (3.71 eV [40], 3.75 eV [47], and 3.79 eV [11]). The difference between the results comes from several sources. The present code uses pseudopotentials and LDA with real-space grid representation, while the calculations in Refs. [11,40] are based on all-electron codes with the BLYP functional. The computation in Ref. [47] is also based on LDA but uses Daubechies wavelets, significantly reducing the effect of the coarseness of the real-space grid (e.g., eggbox effect). The most important source of the difference is that in our real-space grid approach, the weight function is not represented in the same way as in the other approaches using the Voronoi grid [48] or wavelets.

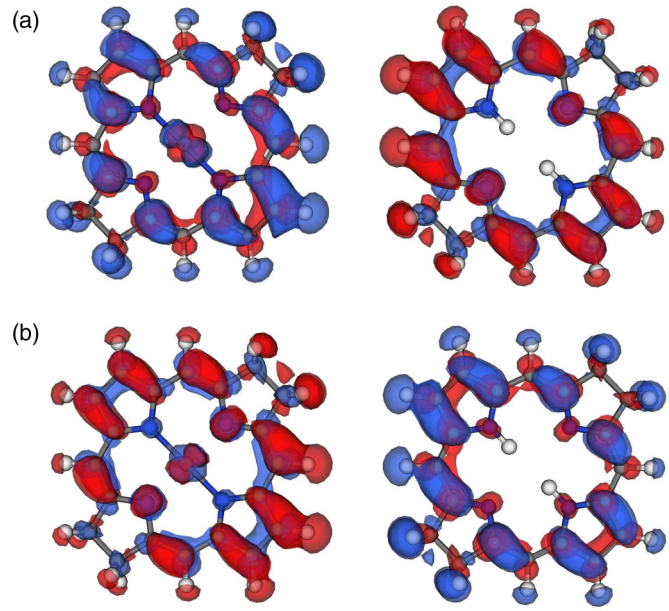

FIG. 5. Density difference between a ground-state DFT calculation of ZnBC-BC and charge constrained DFT representing (a) $ZnBC^+$–BC^- and (b) $ZnBC^-$–BC^+. One isosurface corresponding to densities of 0.006 $Å^{-3}$ is shown. Red (blue) indicates positive (negative) values.

C. Density constraint

The approach can be extended to more general constraints as well. In this section, we demonstrate the ability of the present approach to constrain the spatial density, requiring that $\rho(\mathbf{r})$ is equal to a given value, $Q_0(\mathbf{r}) = \rho_0(\mathbf{r})$. In this case, the operator

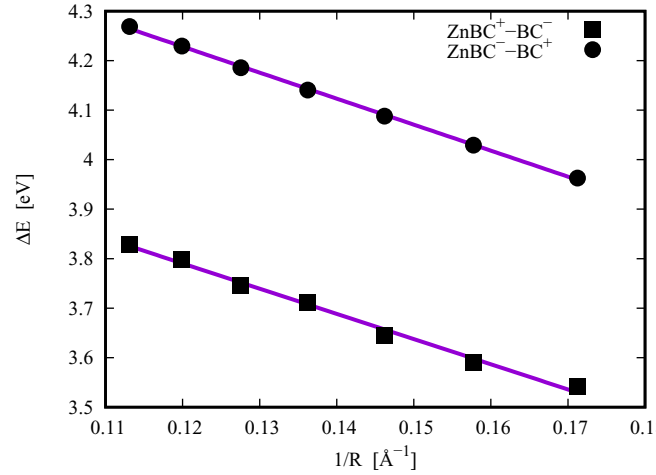

FIG. 6. Total-energy calculations using charge difference constrained DFT to describe the systems $ZnBC^+$–BC^- and $ZnBC^-$–BC^+ for seven separation distances $\mathbf{R}$ chosen at equal increments within a range of 5.84 to 8.84 Å.

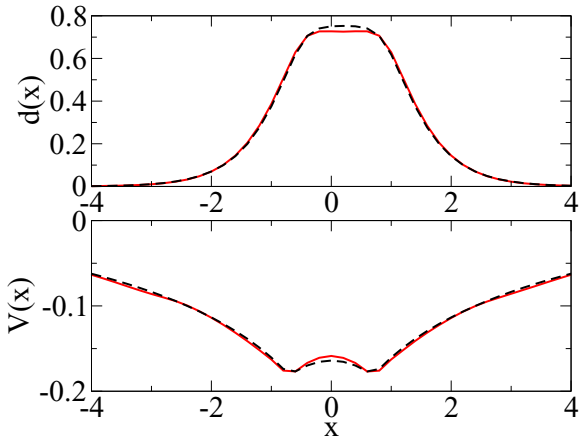

FIG. 7. Top: Exact (solid red line) and DFT (dashed black line) average density $d(x)$ along the x axis connecting the protons. Bottom: cDFT (solid red line) and DFT (dashed black line) average potential $V(x)$ along the x axis. Atomic units are used.

$\hat{Q}$ becomes the density operator such that

$$\left\langle \psi_j^{(n)} \middle| \hat{Q} \middle| \psi_j^{(n)} \right\rangle = \left| \psi_j^{(n)}(\mathbf{r}) \right|^2 \tag{22}$$

and

$$\lambda \hat{Q} \psi_j^{(n)} = \lambda(\mathbf{r}) \psi_j^{(n)}(\mathbf{r}). \tag{23}$$

Given a desired initial density distribution $\rho_0(\mathbf{r})$ and using the steps defined in Eqs. (14), (16), and (17), one looks for the potential $\lambda(\mathbf{r})$, which generates the Kohn-Sham orbitals, $\psi_j^{(n)}$, so that

$$\sum_j \left| \psi_j^{(n)}(\mathbf{r}) \right|^2 = \rho_0(\mathbf{r}). \tag{24}$$

As a first example, we use a simple system, i.e., the H_2 molecule. Fixing the protons at 0.74 Å apart, the two-electron Coulomb problem can be solved very accurately using the variational method with explicitly correlated Gaussian basis functions [49]. The calculated "exact" electron density, shown in Fig. 7, will be the target density $\rho_0(\mathbf{r})$. Figure 7 compares ρ_0 to the density obtained by a conventional DFT calculation. The two densities differ mostly in the middle region between the two protons where the DFT density is higher. Using the density constraint, we then instruct the DFT density to be equal to $\rho_0(\mathbf{r})$. The asymptotic fall of the density is also different, but that is not so important for this test case. The cDFT calculation constrains the density to satisfy $\max|\rho_0(\mathbf{r}) - \rho(\mathbf{r})| < 10^{-5}$, and the constrained and exact densities are indistinguishable in Fig. 7. The cDFT potential [the Kohn-Sham potential plus $\lambda(\mathbf{r})$] and the DFT potential are compared in Fig. 7. The main difference is that the cDFT potential is higher in the middle region, pushing out the charge and correcting the difference between the exact and DFT result. In principle, calculations like this can be used to improve exchange-correlation potentials if accurate densities are available. To check the calculation, one can use the resulting $\lambda(\mathbf{r})$ and add it to the Kohn-Sham Hamiltonian as an external potential. The self-consistent solution produces the desired density distribution $\rho_0(\mathbf{r})$.

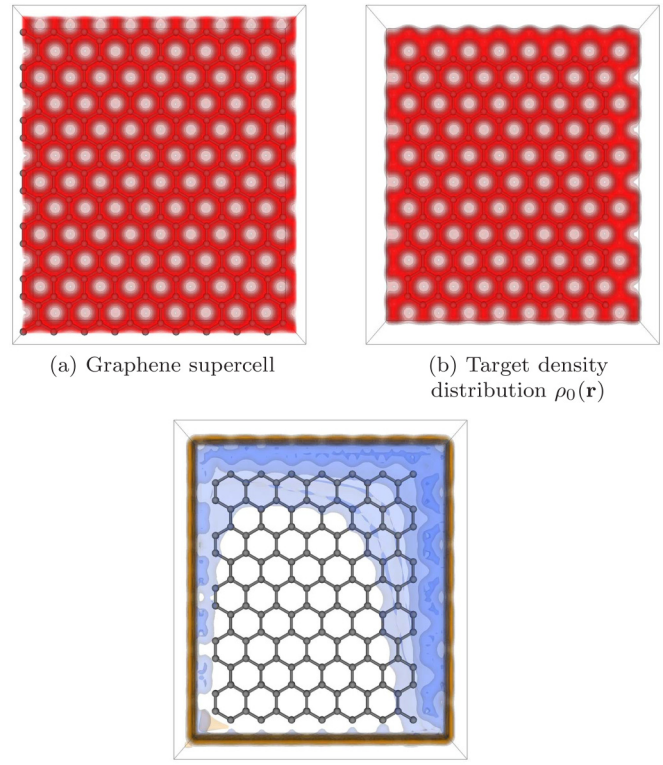

(a) Graphene supercell (b) Target density distribution $\rho_0(\mathbf{r})$

(c) Generated $\lambda(\mathbf{r})$

FIG. 8. Graphene supercell, target density distribution, and $\lambda(\mathbf{r})$ resulting from cDFT. The target density distribution is shown using the graphene fragment molecular geometry used during the cDFT calculation. In depicting $\lambda(\mathbf{r})$, positive (negative) values are represented using orange (blue) isosurfaces.

The next example demonstrates that the approach works for larger systems as well. In this case, we calculate the electron density of a graphene sheet in a periodic supercell calculation, shown in Fig. 8(a). We wish to use this supercell in a finite-box, real-space grid calculation, which requires the density to be zero at the boundary of the grid. To this end, we use a masking function in order to gradually decrease the density to zero at the boundaries and use this distribution as ρ_0. Furthermore, in order to avoid complications arising from atom sites being too close to the boundaries, we prepare a molecular geometry which is exactly the same as the supercell, but with the outer perimeter of atoms removed. This geometry is, then, the atomic coordinates used in the finite-box calculation. The ρ_0 distribution and the modified molecular geometry are presented in Fig. 8(b). Upon initialization, extra Kohn-Sham orbitals are added, beyond those corresponding to the input carbon atoms, in order to ensure that the number of electrons of the initial nonconverged density matches that of ρ_0. We note that because ρ_0 does not necessarily represent an integer number of electrons, there will be one orbital of noninteger occupation. The cDFT generates $\lambda(\mathbf{r})$ [Fig. 8(c)] so that $H_{\mathrm{KS}} + \lambda(\mathbf{r})$ yields $\rho_0(\mathbf{r})$ as the ground-state density. The calculation of a converged constraining potential needs about two to three times more iterations than a conventional DFT iteration. The calculated $\lambda(\mathbf{r})$ can be checked by using it as an external potential to produce $\rho_0(\mathbf{r})$.

This example serves to show that the approach is applicable and converges for larger systems as well. One can recognize the formation of potential wells within the shape of $\lambda(\mathbf{r})$ near the perimeter of the graphene fragment which correspond to the carbon atoms missing in the input molecular geometry. In principle, this graphene fragment can be used to study defects without the problem of periodic images, but still keeping the proper density. One can also use the approach to embed a smaller system into a larger system with density constraints at the boundary. In Ref. [50], charge densities in a boundary region between the two domains have been connected using cDFT to facilitate multiscale calculations using a single scalar λ Lagrange multiplier. The present approach offers a more flexible embedding possibility.

IV. CONCLUSION

We have implemented an iterative optimization approach for constrained density functional calculations. In this approach, the energy minimization and the optimization of the Lagrange multipliers enforcing the constraint are simultaneously iterated. The ideal Lagrange multipliers are determined by enforcing the constraint on the Kohn-Sham orbitals at each self-consistent iteration steps.

The accuracy and efficiency of the present approach is demonstrated on previously studied systems. Comparing the computational cost to previous methods based on the direct optimization of the Lagrange multiplier [11], the present approach is expected to be competitive.

The method is not limited to charge constraints where only a single (or a small set of) Lagrange multiplier is optimized. We have shown that one can prescribe a general, spatially varying density, and the external potential that generates this density as a ground state can be calculated. The applicability of this approach to calculate a spatially dependent $\lambda(\mathbf{r})$ Lagrange multiplier may open up possibilities of embedding smaller systems into larger systems, prescribing boundary conditions using density, or enforcing orthogonality to a given ground state.

ACKNOWLEDGMENTS

The work of A.S.U. was supported by U.S. Department of Energy Grant No. DE-SC0013847.

APPENDIX A: IMAGINARY-TIME PROPAGATION

In this appendix, for completeness of the presentation, we show how the popular steepest-descent iteration can be derived from the imaginary-time step propagation [51]. The important part of this step is that although we only used, to lowest order, the simplest iteration, systematic improvement is possible by including higher-order terms. The origin of the imaginary-time propagation name comes from the similarity of each optimization step and the solution to the time-dependent Kohn-Sham equation,

$$i\hbar\frac{\partial}{\partial t}\psi_k(\mathbf{r},t)=\hat{H}_{\mathrm{KS}}\psi_k(\mathbf{r},t), \tag{A1}$$

for short time steps, Δt:

$$\psi_k(\mathbf{r},t+\Delta t)=\exp[-i\hat{H}_{\mathrm{KS}}\Delta t/\hbar]\psi_k(\mathbf{r},t). \tag{A2}$$

For imaginary-time step propagation, one makes the transformation $\Delta t\to -i\Delta t$ and introduces the parameter $x_0=\Delta t/\hbar$ such that the procedure takes the form

$$\psi_j^{(n+1)}(\mathbf{r})=\exp[-x_0\hat{H}_{\mathrm{KS}}]\psi_j^{(n)}(\mathbf{r}). \tag{A3}$$

Here, we have replaced the notation of our employed wave functions so that they now represent arbitrary functions which are iteratively being updated and approaching the ground-state eigenfunctions of ψ_k. This is seen by noting that such an arbitrary function at iteration n, $\psi_k^{(n)}$, may be expanded as a linear combination of the eigenfunctions of $\hat{H}_{\mathrm{KS}}$,

$$\psi_j^{(n)}=\sum_k c_{j,k}^{(n)}\phi_k. \tag{A4}$$

By plugging this expansion into Eq. (A3), one obtains

$$\psi_j^{(n+1)}(\mathbf{r})=\sum_k c_{j,k}^{(n)}\exp\left[-x_0\epsilon_j^{(n)}\right]\phi_k(\mathbf{r}), \tag{A5}$$

and notes that repeated action by the exponential factor will effectively screen out high-energy contributions. Thus, if orthonormalization is enforced after each iteration via the Gram-Schmidt procedure, the functions $\psi_j^{(n)}$ will converge to the ground-state Kohn-Sham orbitals. Equation (A3) is often further modified by extracting an arbitrary phase factor from each wave function which is related to their associated Hamiltonian eigenvalue,

$$\psi_j^{(n+1)}(\mathbf{r})=\exp\left[-x_0\left(\hat{H}_{\mathrm{KS}}-\epsilon_j^{(n)}\right)\right]\psi_j^{(n)}(\mathbf{r}). \tag{A6}$$

In practice, one may approximate the exponential by its first-order Taylor expansion,

$$\psi_j^{(n+1)}(\mathbf{r})=\mathcal{O}\left\{\psi_j^{(n)}(\mathbf{r})-x_0\left(\hat{H}_{\mathrm{KS}}-\epsilon_j^{(n)}\right)\psi_j^{(n)}(\mathbf{r})\right\}. \tag{A7}$$

Here, $\mathcal{O}$ indicates Gram-Schmidt orthonormalization, which is required to preserve the orthonormality of the single-particle states at each update step.

We note that in order to carry out this procedure, one only requires the action of $\hat{H}_{\mathrm{KS}}$ upon a wave function, as opposed to needing to store a large matrix. In practice, the damping constant x_0 may be replaced with a generalized damping matrix, $D(E_0)$ [52]. Several choices of this operator have been investigated [53]. That used in this work is of the form

$$D(E_0)=\left[1+\frac{T}{E_0}\right]^{-1}, \tag{A8}$$

where T is the kinetic-energy matrix and E_0 is a numeric constant. A good choice for the latter is the depth of the effective Kohn-Sham potential. In this work, determining the action of the damping matrix at each update step, a problem of the form $\vec{y}=D\vec{x}$ is approximately solved by applying a small number of conjugate gradient steps to the equation $[1+\frac{T}{E_0}]\vec{y}=\vec{x}$.

APPENDIX B: CONSTRAINED SYSTEM

1. Lagrange multiplier approach

We restrict the discussion for a single orbital—the extension for many orbitals by requiring orthogonality is simple. We assume that the wave function is expanded in terms of basis functions,

$$\psi(\mathbf{r}) = \sum_{j=1}^{K} c_j \phi_j(\mathbf{r}). \tag{B1}$$

If if one uses a real-space grid, with the basis

$$\phi_i(\mathbf{r}_k) = \delta_{ik}, \tag{B2}$$

where $\mathbf{r}_k$ is a grid point, then

$$\psi(\mathbf{r}_k) = c_k. \tag{B3}$$

We define the matrix elements of the Hamiltonian,

$$H_{ij} = \langle \phi_i | \hat{H} | \phi_j \rangle, \tag{B4}$$

overlap,

$$O_{ij} = \langle \phi_i | \phi_j \rangle, \tag{B5}$$

and constraining operator,

$$Q_{ij} = \langle \phi_i | \hat{Q} | \phi_j \rangle. \tag{B6}$$

Using these matrix elements, the energy is

$$E = \sum_{i,j=1}^{K} c_i c_j H_{ij}, \tag{B7}$$

the norm of the wave function is

$$O = \sum_{i,j}^{K} c_i c_j O_{ij}, \tag{B8}$$

and the constraint is

$$Q = \sum_{i,j=1}^{K} c_i c_j Q_{ij}. \tag{B9}$$

One can now define the functional

$$L(c, \lambda, \nu) = E + \lambda(Q - Q_0) + \nu(O - 1), \tag{B10}$$

where ν and λ are Lagrange multipliers which enforce the normalization and the desired value of Q, respectively. Taking the derivative of L with respect to c, ν, and λ we get the familiar equations

$$\frac{\partial L}{\partial c_j} = \sum_k H_{jk} c_k + \nu \sum_k O_{jk} c_k + \lambda \sum_k Q_{jk} c_k = 0, \tag{B11}$$

$$\frac{\partial L}{\partial \nu} = O - 1 = 0, \tag{B12}$$

$$\frac{\partial L}{\partial \lambda} = Q - Q_0 = 0. \tag{B13}$$

These equations determine the extremal values of c and the values of λ and ν. The actual calculation of these values, however, is not simple. Without the constraint, given by Eq. (B13), Eq. (B11) is a generalized eigenvalue problem and by solving it one obtains the energy eigenvalues and orthogonal orbitals. With the constraint, Eq. (B11) is not a solvable algebraic system (except maybe if $\hat{H}$ and $\hat{Q}$ commute and have a common set of eigenfunctions). One possible solution is to assume some value of λ and try to iterate so that the constraint is fulfilled.

Note, however, that the extremal value of c is not necessarily a maximum or minimum of L. To ensure the minimum or maximum, one has to define [54]

$$L_{ij} = \frac{\partial L}{\partial c_i c_j} = H_{ij} + \nu A_{ij} + \lambda Q_{ij}, \tag{B14}$$

$$o_i = \sum_j O_{ij} c_j, \tag{B15}$$

$$q_i = \sum_j Q_{ij} c_j, \tag{B16}$$

and investigate the determinant

$$\det(e) = \begin{vmatrix} \ddots & & & \vdots & \vdots \\ & L_{ij} - e\delta_{ij} & & o_i & q_i \\ & & \ddots & \vdots & \vdots \\ \cdots & o_j & \cdots & 0 & 0 \\ \cdots & q_j & \cdots & 0 & 0 \end{vmatrix} = 0. \tag{B17}$$

The expansion of $\det(e)$ is a polynomial of the order of $K - 2$. The roots of the polynomial are all positive if E is a minimum at c, and are all negative if E is a maximum at c. Without the constraint, given by Eq. (B13), this polynomial can be used to prove the Ritz variational upper bounds [55].

Even if we would be able to determine c using Eq. (B11), it is not guaranteed that the energy would be minimized. Section B 4 of this appendix details how the energy minimization and the determination of the Lagrange multipliers can be done simultaneously.

2. The approach of Wu and Van Voorhis

Wu and Van Voorhis introduced an approach [11] in which Eq. (B11), the eigenvalue problem of the Kohn-Sham Hamiltonian, is solved for a given λ value. This λ is determined by minimizing

$$f(\lambda) = Q - Q_0 = 0 \tag{B18}$$

by a root-finding algorithm. One can, for example, use a Newton iteration

$$\lambda^{(n)} = \lambda^{(n-1)} - \alpha \frac{f(\lambda)}{f'(\lambda^{(n-1)})}, \tag{B19}$$

where

$$f'(\lambda) = \frac{df(\lambda)}{d\lambda} \tag{B20}$$

and α is the step size. The derivative f' can be calculated using perturbation theory [11] or by finite differencing. In the latter case,

$$f'(\lambda) = \frac{f(\lambda + \delta) - f(\lambda)}{\delta} \tag{B21}$$

has to be calculated for some small δ self-consistently. In this approach, each energy-minimizing self-consistent loop has an inner loop to find λ.

3. Simple iterative optimization

In this section, we describe the iterative optimization of λ. We drop the constraint of the normalization ($\nu = 0$) and consider only the solution of Eqs. (B11) and (B13). For a single orbital, the normalization will be enforced by normalizing the wave function at each iteration; in the case of a set of orbitals, a Gram-Schmidt orthogonalization step will be incorporated.

The simplest iterative solution is a steepest-descent approach where c varies in the direction of the antigradient,

$$c_k^{(n+1)} = c_k^{(n)} - x_0 \frac{\partial L}{\partial c_k} = c_k^{(n)} - x_0 \left[\sum_j (H_{kj} + \lambda Q_{kj}) c_j \right], \tag{B22}$$

and λ changes in the direction of the gradient,

$$\lambda^{(n+1)} = \lambda^{(n)} + x_0 \frac{\partial L}{\partial \lambda} = \lambda^{(n)} + x_0 (Q - Q_0). \tag{B23}$$

This is very closely related to the approach of Wu and Van Voorhis; Eq. (B22) is a self-consistent minimization step and Eq. (B23) steers λ toward the optimal value. The step in Eq. (B23) can be further improved by using f' as in Eq. (B19), if f' is readily available.

4. Constrained iterative optimization

Alternatively, one can adjust λ to fulfill the constraint. Unlike the simple update of λ described in the previous section, now we force the constraint on the interaction. Rewriting Eq. (B22) in matrix vector notation,

$$c^{(n+1)} = c^{(n)} - x_0 (H + \lambda Q) c^{(n)}, \tag{B24}$$

the constraint can be written as

$$\begin{aligned} Q_0 &= c^{(n+1)} Q c^{(n+1)} \\ &= \{[I - x_0 (H + \lambda Q)] c^{(n)}\} Q \{[I - x_0 (H + \lambda Q)] c^{(n)}\}, \end{aligned} \tag{B25}$$

where for the left multiplication one uses the transpose of the vector. Here we omit the transpose sign to simplify the notation. After dropping the terms that are quadratic in x_0, we can solve the equation for λ,

$$\lambda = \frac{1}{c^{(n)} Q^2 c^{(n)}} \left[(c^{(n)} H Q c^{(n)}) - \frac{c^{(n)} Q c^{(n)} - Q_0}{2 x_0} \right], \tag{B26}$$

and use this new λ value in the iteration. This expression contains Q^2 and HQ operators which are simple to evaluate in real-space approaches but could cause difficulties in other basis function representations.

Alternatively [34,35], we can make an iteration for λ in each step, adjusting it to improve the satisfaction of the constraint. We are looking for the optimal $\delta\lambda$ so that the iteration

$$\lambda^{(n+1)} = \lambda^{(n)} + \delta\lambda \tag{B27}$$

converges to the optimal λ value.

The effect of an iterative step using $\delta\lambda Q$ alone is

$$c^{(n+1)} = c^{(n)} - x_0 \delta\lambda Q c^{(n)}. \tag{B28}$$

The same procedure as above gives

$$\delta\lambda = \frac{c^{(n)} Q c^{(n)} - Q_0}{2 x_0 c^{(n)} Q^2 c^{(n)}} \tag{B29}$$

as the optimal $\delta\lambda$ to enforce $Q_0 = c^{(n+1)} Q c^{(n+1)}$. The same approach can also be used to constrain the change of the expectation value of Q. In this case, $\delta\lambda$ should be chosen as

$$\delta\lambda = \frac{c^{(n)} Q c^{(n)} - c^{(n+1)} Q c^{(n+1)}}{2 x_0 c^{(n)} Q^2 c^{(n)}}. \tag{B30}$$

In practice [34,35], the following update algorithm proved to be efficient:

(1) Make an intermediate step,

$$c^{(n+1/2)} = c^{(n)} - x_0 (H + \lambda^{(n)} Q) c^{(n)}. \tag{B31}$$

(2) Change λ to the ideal value,

$$\begin{aligned} \lambda^{(n+1)} = \lambda^{(n)} &+ c_0 \frac{c^{(n+1/2)} Q c^{(n+1/2)} - c^{(n)} Q c^{(n)}}{2 x_0 c^{(n)} Q^2 c^{(n)} + d_0} \\ &+ \frac{c^{(n)} Q c^{(n)} - Q_0}{2 x_0 c^{(n)} Q^2 c^{(n)} + d_0}. \end{aligned} \tag{B32}$$

(3) Advance iteration with the corrected λ,

$$c^{(n)} = c^{(n+1/2)} - x_0 (\lambda^{(n+1)} - \lambda^{(n)}) Q c^{(n+1/2)}. \tag{B33}$$

In step (2), both correction terms [Eqs. (B29) and (B30)] are used: the first one reduces the change in the expectation value and the second one adjusts the expectation value to its desired value. The numerical parameter c_0 sets the relative weight of the two terms. The second numerical constant d_0 is a parameter to compensate the neglected terms in deriving Eqs. (B29) and (B30). In step (3), Q is multiplied by $(\lambda^{(n+1)} - \lambda^{(n)})$ and not by $\lambda^{(n+1)}$ because the $\lambda^{(n)} Q$ term has already acted on the wave function in step (1).

The extension of the above formalism for the many-orbital case is straightforward and the relevant equations are given in the main text.

[1] P. Hohenberg and W. Kohn, Phys. Rev. **136**, B864 (1964).

[2] P. H. Dederichs, S. Blügel, R. Zeller, and H. Akai, Phys. Rev. Lett. **53**, 2512 (1984).

[3] R. Podloucky, R. Zeller, and P. H. Dederichs, Phys. Rev. B **22**, 5777 (1980).

[4] R. van Leeuwen and E. J. Baerends, Phys. Rev. A **49**, 2421 (1994).

[5] Q. Zhao, R. C. Morrison, and R. G. Parr, Phys. Rev. A **50**, 2138 (1994).

[6] Q. Wu, P. W. Ayers, and Y. Zhang, J. Chem. Phys. **131**, 164112 (2009).

[7] H. Akai, S. Blügel, R. Zeller, and P. H. Dederichs, Phys. Rev. Lett. **56**, 2407 (1986).

[8] Z. Zhang and S. Satpathy, Phys. Rev. B **44**, 13319 (1991).

[9] B. Újfalussy, X.-D. Wang, D. M. C. Nicholson, W. A. Shelton, G. M. Stocks, Y. Wang, and B. L. Györffy, J. Appl. Phys. **85**, 4824 (1999).

[10] O. V. Prezhdo, J. T. Kindt, and J. C. Tully, J. Chem. Phys. **111**, 7818 (1999).

[11] Q. Wu and T. Van Voorhis, Phys. Rev. A **72**, 024502 (2005).

[12] H. Eshuis and T. van Voorhis, Phys. Chem. Chem. Phys. **11**, 10293 (2009).

[13] Q. Wu, C.-L. Cheng, and T. V. Voorhis, J. Chem. Phys. **127**, 164119 (2007).

[14] A. M. Souza, I. Rungger, C. D. Pemmaraju, U. Schwingenschloegl, and S. Sanvito, Phys. Rev. B **88**, 165112 (2013).

[15] J. Řezáč, B. Lévy, I. Demachy, and A. de la Lande, J. Chem. Theory Comput. **8**, 418 (2012).

[16] P. Ramos and M. Pavanello, Phys. Chem. Chem. Phys. **18**, 21172 (2016).

[17] H. Oberhofer and J. Blumberger, J. Chem. Phys. **131**, 064101 (2009).

[18] P. Ghosh and R. Gebauer, J. Chem. Phys. **132**, 104102 (2010).

[19] P.-W. Ma and S. L. Dudarev, Phys. Rev. B **91**, 054420 (2015).

[20] A. M. P. Sena, T. Miyazaki, and D. R. Bowler, J. Chem. Theory Comput. **7**, 884 (2011).

[21] L. E. Ratcliff, L. Grisanti, L. Genovese, T. Deutsch, T. Neumann, D. Danilov, W. Wenzel, D. Beljonne, and J. Cornil, J. Chem. Theory Comput. **11**, 2077 (2015).

[22] M. Melander, E. Ö. Jónsson, J. J. Mortensen, T. Vegge, and J. M. García Lastra, J. Chem. Theory Comput. **12**, 5367 (2016).

[23] B. Kaduk, T. Kowalczyk, and T. Van Voorhis, Chem. Rev. **112**, 321 (2012).

[24] N. Holmberg and K. Laasonen, J. Chem. Theory Comput. **13**, 587 (2017).

[25] Q. Wu and T. Van Voorhis, J. Chem. Theory Comput. **2**, 765 (2006).

[26] M. Segal, M. Singh, K. Rivoire, S. Difley, T. Van Voorhis, and M. A. Baldo, Nat. Mater. **6**, 374 (2007).

[27] D. H. P. Turban, G. Teobaldi, D. D. O'Regan, and N. D. M. Hine, Phys. Rev. B **93**, 165102 (2016).

[28] S. Difley and T. Van Voorhis, J. Chem. Theory Comput. **7**, 594 (2011).

[29] S. R. Yost, J. Lee, M. W. B. Wilson, T. Wu, D. P. McMahon, R. R. Parkhurst, N. J. Thompson, D. N. Congreve, A. Rao, K. Johnson, M. Y. Sfeir, M. G. Bawendi, T. M. Swager, R. H. Friend, M. A. Baldo, and T. Van Voorhis, Nat. Chem. **6**, 492 (2014).

[30] J. S. Evans, C.-L. Cheng, and T. Van Voorhis, Phys. Rev. B **78**, 165108 (2008).

[31] J. Behler, B. Delley, K. Reuter, and M. Scheffler, Phys. Rev. B **75**, 115409 (2007).

[32] F. A. Evangelista, P. Shushkov, and J. C. Tully, J. Phys. Chem. A **117**, 7378 (2013).

[33] C. P. Plaisance, R. A. van Santen, and K. Reuter, J. Chem. Theory Comput. **13**, 3561 (2017).

[34] R. Y. Cusson, P. G. Reinhard, M. R. Strayer, J. A. Maruhn, and W. Greiner, Z. Phys. A **320**, 475 (1985).

[35] A. S. Umar, M. R. Strayer, R. Y. Cusson, P.-G. Reinhard, and D. A. Bromley, Phys. Rev. C **32**, 172 (1985).

[36] D. D. O'Regan and G. Teobaldi, Phys. Rev. B **94**, 035159 (2016).

[37] N. Troullier and J. L. Martins, Phys. Rev. B **43**, 1993 (1991).

[38] H. Oberhofer and J. Blumberger, J. Chem. Phys. **133**, 244105 (2010).

[39] F. L. Hirshfeld, Theor. Chim. Acta **44**, 129 (1977).

[40] A. Dreuw and M. Head-Gordon, J. Am. Chem. Soc. **126**, 4007 (2004).

[41] Y. Yamaguchi, S. Yokoyama, and S. Mashiko, J. Chem. Phys. **116**, 6541 (2002).

[42] R. Kobayashi and R. D. Amos, Chem. Phys. Lett. **420**, 106 (2006).

[43] Y. M. Rhee and M. Head-Gordon, J. Phys. Chem. A **111**, 5314 (2007).

[44] I. Duchemin, T. Deutsch, and X. Blase, Phys. Rev. Lett. **109**, 167801 (2012).

[45] A. D. Becke, Phys. Rev. A **38**, 3098 (1988).

[46] C. Lee, W. Yang, and R. G. Parr, Phys. Rev. B **37**, 785 (1988).

[47] L. E. Ratcliff, L. Genovese, S. Mohr, and T. Deutsch, J. Chem. Phys. **142**, 234105 (2015).

[48] F. G. Celia, H. Jan-Willem, B. E. Jan, and B. F. Matthias, J. Comput. Chem. **25**, 189 (2003).

[49] J. Mitroy, S. Bubin, W. Horiuchi, Y. Suzuki, L. Adamowicz, W. Cencek, K. Szalewicz, J. Komasa, D. Blume, and K. Varga, Rev. Mod. Phys. **85**, 693 (2013).

[50] X. Zhang, G. Lu, and W. A. Curtin, Phys. Rev. B **87**, 054113 (2013).

[51] K. Davies, H. Flocard, S. Krieger, and M. Weiss, Nucl. Phys. A **342**, 111 (1980).

[52] C. Bottcher, M. R. Strayer, A. S. Umar, and P.-G. Reinhard, Phys. Rev. A **40**, 4182 (1989).

[53] P.-G. Reinhard and R. Cusson, Nucl. Phys. A **378**, 418 (1982).

[54] H. Hancock, *Theory of Maxima and Minima* (Dover, New York, 1960).

[55] M. Cohen and T. Feldmann, J. Phys. A: Gen. Phys. **4**, 761 (1971).